GYROKINETIC MODELING WITH AN EXTENDED MAGNETIC EQUILIBRIUM INCLUDING THE EDGE REGION OF LARGE HELICAL DEVICE

T. Moritaka
National Institute for Fusion Science
322-6 Oroshi-cho, Toki, 509-5292, Japan
Email: moritaka.toseo@nifs.ac.jp

R. Hager
Princeton Plasma Physics Laboratory
100 Stellarator Road, Princeton, NJ, 08540, USA

M. Cole
Princeton Plasma Physics Laboratory
100 Stellarator Road, Princeton, NJ, 08540, USA

S. Lazerson
Princeton Plasma Physics Laboratory
100 Stellarator Road, Princeton, NJ, 08540, USA

S. Satake
National Institute for Fusion Science
322-6 Oroshi-cho, Toki, 509-5292, Japan

C-S. Chang
Princeton Plasma Physics Laboratory
100 Stellarator Road, Princeton, NJ, 08540, USA

S. Ku
Princeton Plasma Physics Laboratory
100 Stellarator Road, Princeton, NJ, 08540, USA

S. Matsuoka
National Institute for Fusion Science
322-6 Oroshi-cho, Toki, 509-5292, Japan

S. Ishiguro
National Institute for Fusion Science
322-6 Oroshi-cho, Toki, 509-5292, Japan

Abstract

We have developed a gyrokinetic particle-in-cell code toward whole device modeling of Stellarator / Heliotoron. The whole device modeling is needed to investigate long time behavior of plasma transports including core heating and heat exhaust at divertors in a realistic geometry, which is important to estimate the durability of vessel components and design future fusion devices. The simulation code is based on X-point Gyrokinetic Code (XGC) originally developed for Tokamaks. Non-axisymmetric geometries are included by using three dimensional VMEC equilibria. Triangular mesh is generated based on the straight field line coordinate so that the triangle nodes follow magnetic field lines in the toroidal direction. The equilibrium data are extended to the edge region by a virtual casing method and the triangle mesh can be combined with the unstructured mesh numerically generated in the extended equilibrium data. Developed numerical schemes are validated by preliminary benchmark calculations about high-energy particle confinement, GAM oscillation and zonal flow damping.

1. INTRODUCTION

Turbulent and neoclassical transports determine steady-states plasma confinement in the core region of magnetic fusion device. Gyrokinetic simulation is a powerful tool for first-principles approach to describing the transport mechanism. Edge plasma transport also plays an important role in understanding the H-mode transition and the pedestal structure formation [1], edge localized mode crashes, impurity intrusion and heat exhaust to the divertor [2, 3]. In addition, the divertor heat load significantly affects the deterioration of vessel surface. Gyrokinetic simulation code, X-point Gyrokinetic Code (XGC) was originally developed for investigating edge plasma dynamics and core-edge coupling in realistic Tokamak edge geometries [4]. We are now extending XGC to non-axisymmetric Stellarator / Heliotron geometries in which plasma kinetics are poorly

understood in the edge region with stochastic field line structures. In addition, the gyrokinetic approach including finite Larmor radius effect and anisotropic particle motion is effective to investigate roles of stochastic field line structures in the plasma transport.

As the first step, we have demonstrated two typical processes in LHD as preliminary benchmark calculations: (i) GAM oscillation and zonal flow damping in a electric field perturbation and (ii) long-time motion of high-energy particles and particle loss at the material wall. Our results are in agreement with previous studies using separate codes. These two processes, particle loss and GAM oscillation, were demonstrated separately in the previous simulation studies. This is because the core plasma states such as temperature gradient and dynamics accompanied by radial electric fields and zonal flows are well described in flux coordinates while such coordinates are not defined clearly in the edge region. The present simulation scheme including (i) combined use of cylindrical and field-aligned triangle meshes, and (ii) extension of VMEC equilibrium using a virtual casing method, would be promising for whole device gyrokinetic modeling of Stellarators / Heliotrons. We have also investigated particle loss under the effects of ambipolar electric field within the same simulation framework.

This paper is organized as follows: In section 2, we briefly introduce basic numerical procedures in XGC and the numerical schemes newly developed for Stellarators / Heliotrons. Simulation results obtained from the extended code are presented in section 3. Finally, the summary is given in section 4.

2. NUMERICAL SCHEME

XGC employs particle-in-cell method in which plasma dynamics are described by marker particles while perturbed electromagnetic field profiles are given by a spatial mesh. At the present we focus only on electrostatic simulation where magnetic field is constant at an equilibrium state with beta = 0. The marker particles have their own phase valuables (three dimensional space and two dimensional velocity spaces) and are governed by the gyrokinetic equations of motion,

$$\begin{aligned}
\frac{d}{dt}\mathbf{X}_m &= \frac{1}{D}\left(\frac{Ze\rho}{m_i}\mathbf{B} + \frac{1}{Ze|\mathbf{B}|^2}(\mathbf{F}\times\mathbf{B}) + \frac{Ze\rho_m^2}{m_i}(\nabla\times\mathbf{B})\right), \\
\frac{d}{dt}\rho_m &= \frac{1}{D|\mathbf{B}|^2}\left(\frac{1}{Ze}\mathbf{B}\cdot\mathbf{F} + \frac{\rho_m}{Ze}\mathbf{F}\cdot\nabla\times\mathbf{B}\right), \\
\mathbf{F} &= Ze\mathbf{E} - (\mu_m + ((Ze)^2|\mathbf{B}|/m_i)\rho_m^2) \\
D &= 1 + \rho_m(\mathbf{B}/|\mathbf{B}|)\cdot\nabla\times(\mathbf{B}/|\mathbf{B}|)
\end{aligned}$$

where X_{m}, rho_{m} and mu_{m} denote particle position, parallel velocity and magnetic moment, respectively. The electrostatic field is estimated from charge density profiles on mesh vertices interpolated from the spatial distribution of marker particles. The relationship between the electric field and charge density are given by gyrokinetic Poisson equation,

$$\nabla_\perp\cdot\frac{nm_i}{|\mathbf{B}|^2}\nabla_\perp\Phi = Ze\langle\tilde{n}_i\rangle - e\tilde{n}_e,$$

, where phi and n are electrostatic potential and perturbed particle density. To include the edge region, the cylindrical coordinate, rather than the flux coordinates, is used to represent the positions of marker particle. Unstructured meshes adapted to the geometry of fusion device as well as the equilibrium magnetic field [5] are also employed in XGC. The gyrokinetic Poisson equation is solved by using a finite element solver in PETSc library. In addition, hybrid Lagrangian scheme and non-linear collision operator are developed for highly non-thermal dynamics in the edge region [6][7].

In Tokamak cases without resonant magnetic perturbation considered in the original version of XGC, equilibrium magnetic field are axisymmetric and given by a smooth flux function obtained from E-FIT code for the entire region []. For Stellarators, we should consider not only non-axisymmetric three dimensional geometries but also stochastic magnetic field structures in the edge region that can not be defined by flux functions.

We have developed an interface to three dimensional VMEC equilibrium data to include non-axisymmetric magnetic field. The equilibrium data originally defined in a flux coordinate are converted to profile data in the cylindrical and PEST straight field line coordinates. The former is used for particle-mesh interpolation for the magnetic field while the latter is used to generate field-aligned triangular mesh. Positions of the triangle nodes are determined by discretization in the straight field line coordinate. Resulting node positions

in the straight field line coordinate are converted to the cylindrical coordinate in accordance with the VMEC equilibrium data. The rotational transform, iota, as a function of phi is referred in the poloidal discretization so that the triangle nodes follow magnetic field lines in the toroidal direction. The field-aligned triangular mesh could minimize numerical diffusion caused in the particle-mesh interpolation among toroidal cross sections. Figure 1 (right) shows an example of the triangular mesh on a toroidal cross section.

The VMEC equilibrium covers only the core region where the magnetic field has flux surface structures. This equilibrium data are extended to the edge region by using a virtual casing method implemented in STELLOPT library [8, 9]. In this method, edge magnetic field is estimated by the surface current density around the core region as well as the external coil profiles. As a result, a smooth magnetic field profile is obtained for the entire region as shown in Figure 1 (left). Since magnetic field in the core region is identical to the VMEC equilibrium, the triangular mesh is consistent also with the extended magnetic field equilibrium. Triangular mesh in the edge region can not be defined by the flux coordinate but by the numerical field lines tracing in the extended magnetic field equilibrium. Although the meshing schemes and resulting mesh structures are quite different in the core and edge regions, generated meshes can be combined and applied to particle-mesh interpolation and finite element Poisson solver as an unified filed-aligned mesh in the entire region [10].

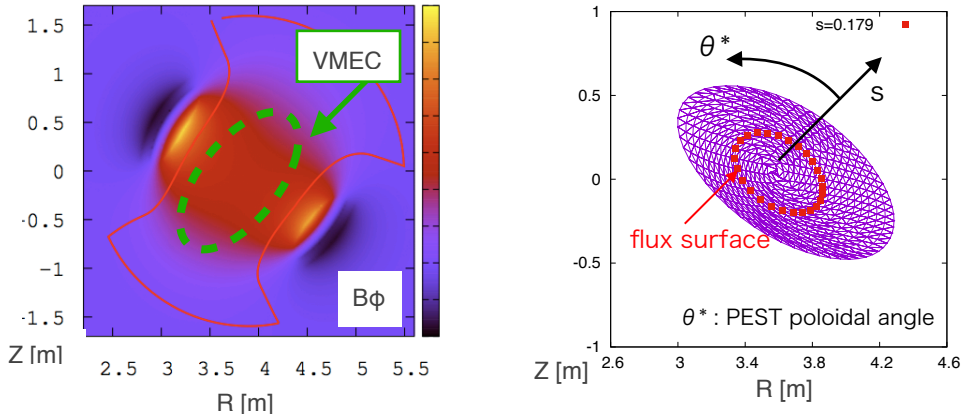

FIG. 1. (left) Profile of magnetic field in the extended magnetic field equilibrium. Core region defined by the original VMEC data is indicated by the green dashed line. Vacuum vessel component inserted is given by the red line. (right) Triangular mesh used for the extended XGC. Resolution is reduced in this figure.

3. SIMULATION RESULTS

The developed code has been verified in two preliminary benchmark calculations for Large Helical Device (LHD). One is particle tracing calculation in the entire region of the extended equilibrium. The other is calculation on GAM oscillation and zonal flow damping using the triangular mesh in the core region. The results are compared with previous studies using separated codes for kinetic simulation for the core region and particle tracing simulation for the entire region.

3.1. ZONAL FLOW DAMPING IN LARGE HELICAL DEVICE

As the first benchmark calculation using the triangular mesh, we simulate collisionless interaction between radial electric field and ion flux in the core region of LHD. We only consider radial electric field averaged over flux surface while three dimensional motions of marker particle are evaluated in the extended equilibrium. Charge density profile is estimated by particle-mesh interpolation on the triangular mesh and time evolution of radial electric field, E_{rho}, are evaluated from

$$(\langle|\nabla\rho|^2|\rangle_\rho + \langle\frac{c^2}{v_A^2}|\nabla\rho|^2\rangle_\rho)\epsilon_0\frac{\partial E_\rho(\rho)}{\partial t} = -eZ_i\langle\Gamma_i\rangle_\rho$$

where, rho, v_{A} and Gamma denote normalized minor radius, Alfven velocity and radial ion flux, respectively. This equation is analytically consistent with the gyrokinetic Poisson equation for a flux averaged electrostatic potential. We introduce perturbed radial electric field and uniform plasma as an initial condition. The electric field perturbation eventually dissipates due to the interaction of ion flux, however, a part of the perturbation remains with a zonal flow in the poloidal direction. This interaction process is considered to be a combination of GAM oscillation and long time behavior characterized by damping rate and residual level [11].

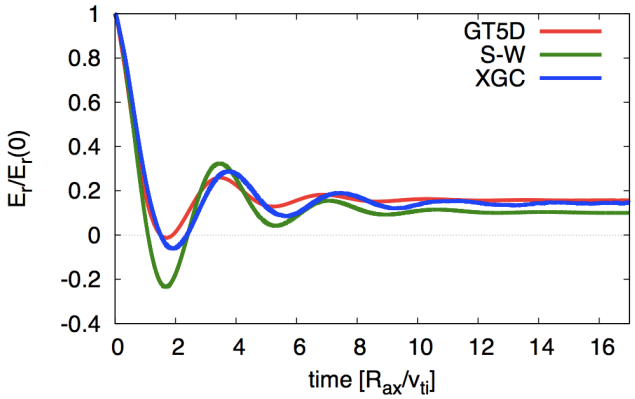

FIG. 2. Time evolution of the radial electric field perturbation normalized to the initial amplitude resulting from XGC (blue) and GT5D (red). These values are sampled at rho = 0.5, where rho is normalized minor radius. Green line denote the analytical formulation derived by Sugama and Watanabe [].

Figure 2 (blue line) shows time evolution of radial electric field obtained from XGC. Amplitude of the electric field is normalized to the initial value, E_{0} = 1 [eV]. This result is in good agreement with that obtained from another gyrokinetic simulation code, GT5D (red line) [12], and the prediction from the analytical formulation [11] (green line). This agreement indicate validity of particle-mesh interpolation on the field-aligned mesh and particle push kernel in the non-axisymmetric system.

The gyrokinetic Poisson equation is not solved in the present benchmark calculations. We have confirmed that the finite element solver is converged on the triangular mesh and resulting potential structure is consistent with the electric field obtained from the one dimensional equations used here [10]. In addition, as a benchmark calculation including finite element Poisson solver, linear growth of ion temperature gradient instability is recently demonstrated for a circular Tokamak in the present framework generalized for non-axisymmetric geometries (M. Cole et al, IAEA FEC 2018).

3.2. HIGH ENERGY PARTICLE CONFINEMENT UNDER RADIAL ELECTRIC FIELDS

Using the extended VMEC equilibrium and the triangular mesh, we investigate high energy particle confinement in LHD under the influence of ambipolar radial electric field. The ambipolar electric field is estimated in a similar manner to the previous benchmark calculation on zonal flow damping. Difference is that we set a non-uniform initial density profile instead of the electric field perturbation. GAM oscillation is observed to be excited and eventually saturated in the ambipolar state with an inward electric field which tends to confine thermal ions in the core region. Although the equilibrium magnetic field employed is different, the GAM frequency (~ ($\sqrt{7}/2$) v_{Ti}/R_{x}) and amplitude of the ambipolar electric field (~ 1 - 10 [kV/m]) obtained here are roughly consistent with the results of the global neoclassical particle code, Fortec-3d [13], where R_{x} and v_{Ti} are the major radius and the ion thermal velocity, respectively.

Particle trajectories are evaluated by the three dimensional version of push kernel in XGC. Extended VMEC equilibrium for the entire region of LHD is used as a background magnetic field. Marker particles are initially placed along the equatorial line on the toroidal cross section with phi = 0 as shown in Fig. 3. Particles are traced until t = 10 [ms] or they are lost at the vacuum vessel, which is implemented from a CAD data. Particle energy is fixed at 25 or 100 [keV]. In this case, initial condition of particle is determined by position and pitch angle. In Stellarator geometries, particle dynamics are classified into three regimes with passing, banana and chaotic orbits. Particles with the chaotic orbit move away from the flux surfaces and are eventually lost at the vacuum vessel. In the absence of the radial electric field, initial conditions for the chaotic orbit and particle loss are in good agreement with the results of the previous simulation study [14]. In that simulation particle orbits were evaluated in magnetic field equilibria obtained for the entire region of LHD by using HINT code with a relaxation scheme without assuming flux surface structures [15].

Figure 3 (top) shows the deviation of flux label along the particle orbit as a function of initial particle position. Green and blue lines stand for the results for 100 and 25 [keV] cases in the absence of the radial electric field, respectively. Purple and orange lines are those in the presence of the radial electric field. The deviation is averaged over the initial pitch angle. In the high energy case, (100 [keB]) the deviation is hardly

changed in the electric field. On the other hand, the deviation in the intermediate energy case (25 [keV]) increases near LCFS ($r < 4.4$ [m]) in the presence of the electric field. This results indicate that the particles are scattered under the influence of the electric field more effectively and tend to move away from the flux surfaces.

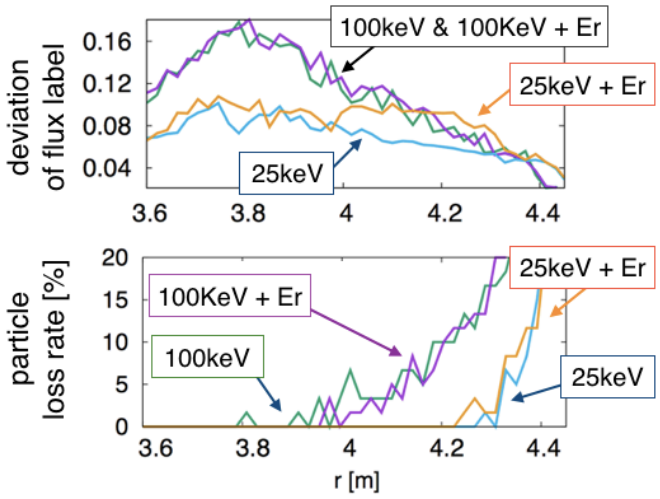

FIG. 3. Deviation of flux label along the particle orbit (top) and particle loss rate (bottom) as functions of initial particle position. These values are averaged over the initial pitch angle.

Figure 3 (bottom) shows particle loss rates averaged over the initial pitch angle as a function of the initial position. One can see that the electric field affects particle loss in two different ways. In the high energy case (100 [keV]), particles tend to be confined in the inward electric field as in the thermal ions. Conversely the electric field causes additional particle loss through the modification of particle trajectory in the intermediate energy range (25 [keV]). Effect of the radial electric field observed here on the particle loss ratio is rather limited within a few %. This is because energy of particles considered here is large compared to the electrostatic potential. The energy-selective effects of radial electric field would become apparent in lower energy range and also affect the characteristics of heat flux to the divertor.

4. SUMMARY

Toward whole device modeling of Stellarator we have developed an extended version of the gyrokinetic particle-in-cell code, XGC, which is originally developed for Tokamaks. Challenging issue for this is to address the non-axisymmetric geometry and complicated edge region without flux surface structures. Three dimensional equilibrium data obtained from VMEC is employed for the core region and extended to the edge region by using a virtual casing method in the cylindrical coordinate. In addition, triangular meshes are generated by discretizing the straight field line coordinate so that the triangle nodes follow magnetic field lines in the toroidal direction. Resulting mesh can be combined with unstructured mesh for the edge region and employed in the finite element Poisson solver.

The implemented schemes have been applied to basic benchmark calculations on radial electric field and high energy particle confinement in Large Helical Device. Time evolutions of radial electric field accompanied by zonal flow damping and GAM oscillation are observed to be consistent with the results of gyrokinetic code, GT5D, and neoclassical code, Fortec-3D. High-energy particle orbits in the extended VMEC equilibrium is also in good agreement with hose obtained in the high-accuracy particle tracing calculation using HINT equilibria. In addition, we have investigated the influence of ambipolar electric field in high-energy particle confinement. It is demonstrated that the radial electric field tends to confine high-energy particles (100 [keV]) as well as thermal plasmas while loss rate of intermediate energy particles (25 [keV]) increases due to disturbance of particle orbit in the radial electric field.

In these primary calculations, we only consider radial electric field and high energy particles. The ambipolar electric field and other neoclassical phenomena could have more significant impact on particle dynamics with lower energies comparable to the potential energy. In future work, we will investigate relationship between neoclassical phenomena in the core region and edge plasma dynamics such as heat flux to the divertors. To estimate particle and heat fluxes in the edge region, we will implement the numerical schemes concerning non-thermal distribution and collisional interaction, i.e., the hybrid-Lagrangian scheme and the

nonlinear collision operator. These are potentially applicable for Stellarator geometries because only particle distribution localized in the real space are considered in these schemes.

.

ACKNOWLEDGEMENTS

This work is performed on "Plasma Simulator" (FUJITSU FX100) of NIFS with the support and under the auspices of the NIFS Collaboration Research program (NIFS16KNSS085). This work was also supported by JSPS KAKENHI Grant Number 16H07419 and Japan / U. S. Cooperation in Fusion Research and Development (JF-5, 2017).

REFERENCES

1. C. Gormezano, A.C.C. Sips, T.C. Luce et al., Nuclear Fusion **47** (2007) S285.
2. R.M. Churchill, J.M. Canik, C.S. Chang et al., Nuclear Materials and Energy **12** (2017) 978.
3. C.S. Chang, S. Ku, A. Loarte et al., Nuclear Fusion **57** (2017) 116023.
4. S. Ku, C. S. Chang and P. Diamond, Nucl. Fusion **49** (2009) 115021.
5. F. Zang, R. Hager, S. Ku et al., Engineering with Computers **32** (2016) 285.
6. S. Ku, R. Hager, C. Chang et al., J. Comput. Phys. **315** (2016) 467.
7. E. S. Yoon and C. S. Chang, Phys. Plasmas **21** (2014) 032503.
8. M. McMillan1 and S. A. Lazerson, Plasma Phys. Control. Fusion **56** (2014) 095019.
9. S. A. Lazerson, Plasma Phys. Control. Fusion **54** (2012) 122002.
10. T. Moritaka, R. Hager, M. Cole et al., in preparation.
11. H. Sugama and T.-H. Watanabe, Phys. Plasmas **13** (2006) 012501.
12. S. Matsuoka, Y. Idomura and S. Satake, Phys. Plasmas **25** (2018) 022510.
13. S. Satake, H. Sugama and T.-H. Watanabe, Nucl. Fusion **47** (2007) 1258.
14. R. Seki, Y. Matsumoto, Y. Suzuki et al., Plasma and Fusion Res. **3** (2008) 016.
15. Y. Suzuki, N. Nakajima, K. Watanabe et al., Nuclear Fusion **46** (2006) L19.